Journal of
Micromechanics and
Microengineering

PAPER • **OPEN ACCESS**

Fluorosilane-induced softening and collapse of micropillar arrays

To cite this article: Gabriela Moreira Lana *et al* 2025 *J. Micromech. Microeng.* **35** 115009

OPEN ACCESS
IOP Publishing
Journal of Micromechanics and Microengineering
J. Micromech. Microeng. **35** (2025) 115009 (12pp)
https://doi.org/10.1088/1361-6439/ae1e87

Fluorosilane-induced softening and collapse of micropillar arrays

Gabriela Moreira Lana[1,2,5], Maja Fehlberg[1,3,5], Petra Herbeck-Engel[1], Gisela Heppe[1], Raimund Schlüßler[4], Torsten Jähnke[4], Eduard Arzt[1] and Roland Bennewitz[1,3,*]

[1] INM—Leibniz Institute for New Materials, Campus D2 2, 66123 Saarbrücken, Germany
[2] Polymer Science and Engineering Department, University of Massachusetts Amherst, Amherst, MA 01003, United States of America
[3] Saarland University, Physics Department, Campus 66123 Saarbrücken, Germany
[4] CellSense Technologies GmbH, 12489 Berlin, Germany

E-mail: roland.bennewitz@leibniz-inm.de

Received 19 September 2025, revised 21 October 2025
Accepted for publication 12 November 2025
Published 24 November 2025

Abstract

Replica molding is a widely used technique for the fabrication of polymer microstructures. As structural dimensions decrease, anti-stick surface treatment of the mold becomes increasingly critical to ensure clean demolding and preserve structural integrity. We fabricated arrays of micropillars with 20 μm diameter and 60 μm height using medical-grade polydimethylsiloxane (PDMS), MDX4-4210, and observed a high fraction of collapsed pillars for the first molding after fluorosilanization of the mold to reduce sticking. To address this issue, we systematically investigated the surface treatment protocol for the molds, made from the PDMS Sylgard 184. We provide results from complementary measurement methods, to show that an additional vacuum step partially removes unbound fluorosilane, but does not improve pillar stability. In contrast, a method based on multiple replications, where the first replication effectively removes residual fluorosilane from the mold, significantly enhances structural stability. Mechanical testing further revealed that the presence of fluorosilane lowers the Young's modulus of both PDMS materials, MDX4-4210 and Sylgard 184, suggesting interference with the curing process. Confocal Brillouin microscopy indicated an elongation of replicated pillars and revealed a softening close to the surfaces, as well as mechanical inhomogeneities in collapsed pillars. We discuss modifications to the molding protocol to improve the reproducibility and mechanical stability of the replicated microstructures, offering insights towards more reliable routes for the fabrication of residue-free, high-aspect ratio features with controlled surface chemistry.

[5] These authors contributed equally to this work.
[*] Author to whom any correspondence should be addressed.

Supplementary material for this article is available online

Keywords: microstructure, PDMS, replica molding, anti-stick coating, fluorosilane, surface treatment

1. Introduction

Micropatterning of surfaces is a powerful tool to create and tune materials functionalities by changing their architectures [1]. A versatile material for the fabrication of microstructured devices is polydimethylsiloxane (PDMS), which can be patterned for a plethora of applications from dry, reversible adhesives [2–4] to flexible devices [5], from microfluidics [6] to lab-on-a-chip technologies [7, 8], and in biomedical research, from skin applications [9, 10] to tissue engineering [11].

Replica molding is an important fabrication technique for polymeric devices and microstructures [12]. It yields numerous precise copies from one single master sample. Therefore, two substantial advantages emerge: (i) fewer master samples are needed, reducing costly and time-consuming fabrication; and (ii) the lifetime of the original master structure is increased since its negative replica is used repeatedly instead [13, 14]. The deposition of anti-stiction coating through the vapor phase is a routine process step in replica molding [15, 16]. It allows the secure separation of the materials by a simple and inexpensive method [17, 18]. Fluorinated silanes are often used to generate a hydrophobic, anti-stick surface. For instance, a standard coating is the fluorinated trichlorosilane (tridecafluoro-1,1,2,2-tetrahydrooctyl) trichlorosilane (AB111444, ABCR, Karlsruhe, Germany) hereafter referred to simply as fluorosilane), in which a long hydrophobic, fluorinated chain is bound to a Si atom surrounded by three chlorine atoms that readily react in the presence of air into OH groups and attach to silicon-containing substrate as siloxane (Si–O–Si) bridges [13, 16, 19–21]. The quality of the fluorosilane layer can be considerably improved by activating the surface with plasma or reducing humidity, affecting the mechanism of fluorosilane layer formation. Plasma treatment is commonly used to introduce hydroxyl groups on the surface, increasing the number of anchoring points for covalent bonding during chemical functionalization [22–25].

However, this method generates an unstable coating with excess material and a limited lifetime [13]. The amount of deposited film is usually not precisely controlled, being regulated mainly through the deposition time at the vapor pressure of the fluorosilane. The thickness of the coating, a few layers of molecules [26], is generally difficult to characterize [19]. The precision of the coating thickness can be critical if the feature size of microstructures is reduced to tens of microns [20]. For example, in the case of fabricating a micropillar array, lateral collapse of slender structures due to the action of surface forces is reported [27]. This effect is undesired for pillar structures used for dry adhesion, as collapsed or bundled fibrils have hindered contact formation with the counter surface.

Previous studies on PDMS micropillar arrays fabricated via soft lithography report structural collapse, which has been addressed through geometric modifications such as reducing aspect ratio or increasing spacing, combined with treatments like ultrasound to recover collapsed pillars [28], demolding inside a solvent [29], post-demolding washing to swell and separate the structures [30], or supercritical CO_2 drying to partially restore epoxy nanopillars [31]. Zhang *et al* further highlighted how material stiffness plays a critical role in structural recovery, underscoring the need for tailored approaches when working with soft elastomers like PDMS. Yet even with these approaches, collapsed pillars are observed as the presence of liquid bridges can still induce collapse [32]. For micropillar fabrication using other methods such as two-photon polymerization, collapse has been mitigated by increasing laser exposure time to enhance crosslinking density [33], applying a post-bake treatment at low temperatures (−50 °C) [34], or by employing stiffer resins [35]. These approaches, however, involve materials with moduli in the GPa range.

To address the challenge of producing structurally intact (i.e. non-collapsed) pillared foils, we used negative molds fabricated from Sylgard 184 PDMS (Dow Silicones, Midland, MI, USA, 10:1 base:curing agent ratio, hereafter referred to simply as Sylgard) and examined the impact of excess fluorosilane on the mold's surface during the curing process of the positive sample covered with pillars made of PDMS MDX4-4210 (Dow Corning Corp, Midland, MI, USA, hereafter referred to simply as MDX4). While this medical grade silicone offers advantages for biomedical applications, the low stiffness of MDX4 (compared to standard Sylgard 184) led to significant fabrication challenges. In this work, we focused on circular cross-sections, which have isotropic bending properties and found application as gecko-inspired dry adhesives [3, 9].

To ensure that our mold treatment strategies are effective for demanding materials, we used the very soft MDX4 to fabricate the pillars. By focusing on these more fragile structures, we aim to develop a broadly applicable solution for improving pillar stability. Moreover, MDX4 is biocompatible, and the resulting foils are suitable for in-vivo studies and medical applications.

We introduce two strategies to improve the stability of the micropillars. The first strategy is to add a vacuum step to the process to remove excess fluorosilane from the molds after the anti-stiction coating. The second strategy involves multiple replication steps, where the first replication removes residual fluorosilane from the mold, resulting in more robust and less deformable pillars in the following replications. Additionally, we examine the influence of plasma treatment prior to fluorosilanization on the microstructure integrity. By

refining these techniques, we aim to achieve more reliable and accurate replica molding for small-scale structures. The effectiveness of the mold fluorosilanization steps is evaluated by complementary characterization methods, covering different physical aspects such as surface energy, chemical composition, structural accuracy, and elasticity.

2. Experimental

2.1. Sample fabrication

Master structures: The master structures consisted of hexagonal arrays of micropillars, each pillar with a diameter of 20 μm and a height of 60 μm, with a distance between pillar centers of 40 μm. Circular cross-sections were chosen for their isotropic bending properties and mechanical robustness during demolding. The aspect ratio of 3:1 for height over diameter was found to be the practical upper limit for fabrication for MDX4 as material and our hexagonal array configuration. The positive design was created in Autodesk Inventor (Autodesk, San Rafael, CA, USA) and an array area of $1.5 \times 1.5\,\text{cm}^2$ or $0.5 \times 0.5\,\text{cm}^2$ was printed on $2.5 \times 2.5\,\text{cm}^2$ silicon wafers using a methacrylate-based resin and a two-photon laser lithography system (Photonic Professional GT, Nanoscribe, Karlsruhe, Germany) with a 25× objective. To promote adhesion between the wafer and the resin, the silicon surface was pretreated with 3-(trimethoxysilyl)propyl methacrylate.

After printing, the structures were developed in propylene glycol monomethyl ether acetate (PGMEA, Sigma-Aldrich, St. Louis, MO, USA) for 60 min, exchanged with isopropanol (Sigma-Aldrich, Steinheim, Germany), and post-cured under UV light for 300 s at 365 nm (OmniCure S1500A, igbtech, Friedelsheim, Germany). Samples were rinsed with isopropanol and dried under airflow. Measurements of 20 randomly selected printed pillars showed an average height of 62.0 ± 0.9 μm and an average diameter of 19.0 ± 1.3 μm.

Negative molds: Negative molds were fabricated by casting Sylgard onto the master structures. Prior to molding, the masters were silanized to form an anti-stick coating. This process involved plasma activation (1 min, Atto low pressure plasma system, Electronic Diener, Ebhausen, Germany) followed by vapor phase deposition of fluorosilane under 3 mbar vacuum for 5 min. The PDMS was degassed, cured at 95 °C for 1 h, and then gently peeled from the master. To avoid any influence of un-crosslinked silicone on the mold treatments and, consequently, on the quality of the replicas, we prepared the Sylgard according to the manufacturer's instructions using a 10:1 base-to-curing agent ratio. With this mixing ratio and curing temperature, the elastic modulus of Sylgard is reported to be approximately 2 MPa [36].

Micropillar array: To fabricate the final micropillar structures, the negative molds were first subjected to defined surface treatments, as described in detail in section 2.2. Following the manufacturer's instructions, the medical grade PDMS MDX4 was mixed with a ratio of 10:1, poured into the treated molds and degassed for 5 min to ensure proper filling of the cavities. The filled molds were spin-coated at 1000 rpm for 120 s (Laurell WS 650 MZ–23NPPB, North Wales, PA, USA) to create a uniform backing layer and then cured at 95 °C for 1 h. After curing, the micropillar arrays were carefully demolded by peeling off the backing layer edges. The procedure is represented in figure 1.

2.2. Surface treatment of the negative mold

To investigate the impact of mold surface chemistry on micropillar fidelity, four different surface treatment protocols were defined, as indicated in figure 1:

- **Group 1:** Fluorosilanization only (no plasma or vacuum).
- **Group 2:** Plasma activation and fluorosilanization (no vacuum).
- **Group 3:** Fluorosilanization followed by a vacuum step (no plasma).
- **Group 4:** Plasma activation, fluorosilanization, and vacuum step.

All molds were coated by vapor deposition of fluorosilane, placing the molds and an open container with liquid fluorosilane for 5 min into a desiccator evacuated to approximately 3 mbar to create an anti-stick coating. The 5 min coating duration was determined based on preliminary optimization experiments. Shorter fluorosilanization times consistently resulted in insufficient anti-stick coating, causing the sample to stay adhered to the mold and preventing clean detachment. Molds from Groups 2 and 4 were activated by air plasma for 1 min prior to the fluorosilanization step. After fluorosilanization, the molds of Group 3 and 4 were placed inside a clean desiccator for 18 min under continuous pumping to a pressure of about 3 mbar, with the intention of removing excess fluorosilane molecules that were not attached to the surface.

2.3. Characterization

Microscopy: Samples were imaged using an optical microscope (Eclipse LV100ND, Nikon, Tokyo, Japan) and a confocal microscope (MarSurf CM explorer, 20× objective, Mahr, Göttingen, Germany). The final pillar structures were evaluated with the Mahrsurf microscope, where 3–10 images of $0.64\,\text{mm}^2$ size were recorded in randomly selected positions for each sample (depending on the base area of the samples). The upright/collapsed pillars of all images were counted to evaluate the fraction of upright pillars.

Water contact angle (WCA): The surface energy throughout the fabrication process was investigated by monitoring the hydrophobicity of Sylgard and MDX4 surfaces submitted to different treatments. To isolate the effects of surface chemistry from structural features, the WCA measurements were carried out on flat Sylgard and MDX4 films that underwent the same surface treatments as the molds and pillar samples.

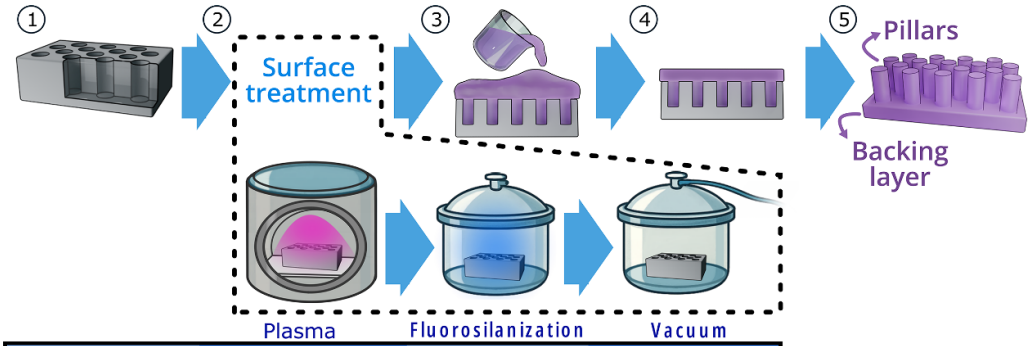

Figure 1. A schematic representation of the fabrication process for MDX4 micropillar arrays. (1) A negative mold is prepared using Sylgard. (2) The mold undergoes surface treatment, which may include plasma activation, vapor-phase deposition of a fluorinated silane, and a vacuum step to remove unbound fluorosilane residues. (3) The pillar-forming material (MDX4) is poured onto the mold. (4) Spin coating is performed to ensure a flat, uniform base layer (backing layer). (5) After curing, the micropillar array is demolded. This study evaluates the effect of different combinations of surface treatment steps by comparing four experimental groups, as indicated in the table: Group 1 (fluorosilanization only), Group 2 (plasma + fluorosilanization), Group 3 (fluorosilanization + vacuum), and Group 4 (plasma + fluorosilanization + vacuum).

First, Sylgard films were prepared by spin coating the polymer on glass substrates, using 400 rpm for 2 min. Plasma, fluorosilanization, and vacuum draw were performed on these films, following the surface treatment in four groups which we adopted for the molds. To emulate the interaction with the fibril material, a MDX4 film was prepared on top of the treated Sylgard film and peeled off after curing in an oven for 1 h at 95 °C. Measuring the mold material before and after one replication step allowed us to assess changes relevant to the fabrication of both the first and second pillar samples. After each step (including the MDX4 detachment), the Sylgard films were immediately tested for their contact angles with a goniometer (OCA 25 DataPhysics Instruments GmbH, Filderstadt, Germany) applying water droplets of 3 μl. The WCA was calculated in sessile mode using the provided software (SCA 20). Each sample was measured at three independent positions and the standard deviation amongst the positions is presented. A schematic representation of the measured films is presented in the supplementary material (SM) in figure S1.

Elastic Modulus: Nanoindentation tests were carried out using a TI 950 device with a Performech controller (Hysitron TriboIndenter, Hysitron Inc. Minneapolis, MN, USA, now Bruker). A spherical sapphire indenter (radius $\sim 400\,\mu$m) was used. All measurements were conducted using displacement control, with both approach and retraction rates set to 200 nm s^{-1}. On pillared surfaces, the elastic modulus E was calculated from the normal stiffness k_1 of single pillars in extension following Guidoni *et al* [37] using equation (1):

$$E = \left(\frac{H}{(1-\nu^2)\,a} + \frac{16}{3\pi}\right)\frac{(1-\nu^2)}{a\pi}k_1 \qquad (1)$$

where a is the radius of the pillars, H their height and $\nu = 0.5$ Poisson's ratio of the MDX4.

For flat surfaces, the Oliver–Pharr method was employed [38], using the first 200 data points after the maximum indentation to determine the slope, thereby minimizing the influence of material adhesion. The elastic modulus was calculated using equation (2)

$$E = \left(1-\nu^2\right)\left(\frac{1}{E_\mathrm{r}} - \frac{\left(1-\nu_i^2\right)}{E_i}\right) \qquad (2)$$

with

$$E_\mathrm{r} = \frac{\sqrt{\pi}}{2}\frac{S}{\sqrt{A_\mathrm{c}}},$$
$$A_\mathrm{c} = \pi\left(2Rh_\mathrm{c} - h_\mathrm{c}^2\right),$$
$$E_i = 1140\,\mathrm{GPa},$$
$$\nu_i = 0.07$$

where h_c is the contact depth, A_c is the contact area between tip and sample, E_r is the reduced modulus and E_i is the elastic modulus of the tip.

Uniaxial compression tests were performed using a universal Testing Machine (UPM, ZwickRoell Model 1446 Retroline) through compression test up to a maximum force of 50 N or a maximum deformation of 10 % with a velocity of 0.5 mm per minute (see figure S2(a) in the SM). For these experiments, we produced cylindrical samples with a diameter of 34 mm and a height of 11.5 mm. The interface between samples and instrument was lubricated by Sylgard 184 Component A oil to avoid barreling of the samples under compression. The modulus was calculated from the slope of

the stress vs. strain with deformation greater than 5% or force greater that 10 N (see figure S2(b) in the SM).

2.3.1. Fourier Transform Infrared (FTIR): The chemical composition of the surfaces and coatings was analyzed with a FTIR spectrometer Tensor 27 from Bruker equipped with ATR accessory (Specac), and the spectra were evaluated using the software LabSpec. Spetra were scaled by CH bands (2962 νCH and 1257 δCH)

2.4. Brillouin microscopy:

Brillouin microscopy was performed to assess the mechanical properties of the micropillars at high spatial resolution [39, 40]. The measurements were conducted using an inverted Brillouin microscope (Discoverer from CellSense, Berlin, Germany) equipped with a 40× C-Apochromat 1.20/W Korr water immersion objective (Zeiss) and a 780.24 nm excitation laser. All measurements were performed in reflection mode (180° scattering angle) at room temperature (20 °C). MDX4 pillar arrays were placed on a 170 μm cover glass with immersion medium (Immersol Sil 406, $n = 1.406$) between the pillars and the cover glass. Two measurement configurations were recorded:

- vertical scan along the axial plane of single pillars, 170 × 59 pixels, 0.7 μm step size
- horizontal scan along the median plane of a group of pillars, 111×111 pixels, 1 μm step size

Brillouin frequency shifts were extracted using spectral fitting of the backscattered light. To reduce the influence of edge effects and confocal overlap between medium and material, measurements were analyzed only at a horizontal distance of 1 μm and a vertical distance of 4 μm from the material–medium interface.

3. Results and discussion

To enable the miniaturization of previously reported fibrillar adhesive structures [2, 41] for application in biomedicine [9, 42], we used the medical grade silicone MDX4 instead of conventional materials such as Sylgard 184. With a Young's modulus of 1.1 MPa [9], the silicone MDX4 is relatively soft, compared to commonly used Sylgard.

We observed initially a high incidence of pillar collapse after demolding, which we attributed to the reduced mechanical stability of MDX4 as relatively long, slender pillars (aspect ratio 3:1), and possible interactions with mold surface chemistry. We hypothesized that the surface treatment of the negative molds plays a critical role in determining pillar stability, with residual anti-stick agents, such as unbound fluorinated silane, potentially interfering with polymer curing or altering surface energy balance.

We first evaluated how the mold surface treatment influenced surface energy, using static WCA measurements on flat Sylgard films subjected to the same sequence of treatments applied to the negative molds, as presented in figure S1 in the SM. The untreated Sylgard exhibited a high contact angle (116°), consistent with its intrinsic hydrophobicity [43, 44]. As expected, plasma activation rendered the surface highly hydrophilic, with the contact angle dropping below 12° [45]. Subsequent fluorosilanization restored hydrophobicity, yielding contact angles above 110°, and these values remained stable after vacuum and demolding steps.

Despite the clear shift from hydrophilic to hydrophobic states after fluorosilanization, we did not observe substantial differences in the final WCA values across treatment groups, particularly after the vacuum step and demolding. These results suggest that static contact angle measurements are not sufficiently sensitive to detect residual unbound fluorosilane on the surface. To gain more detailed insight into the chemical modifications induced by the treatments, we performed FTIR spectroscopy on films subjected to the same surface treatments applied to the negative molds (namely plasma activation, fluorosilanization, vacuum, and fabrication and removal of a MDX4 layer).

In figure 2(a), we observe that plasma treatment increased the number of hydroxyl groups on the surface, as indicated by the growing intensity of the broad OH stretching band (3261 cm^{-1}) [46] from both adsorbed water (3600 cm^{-1}) and Si–OH bonds. This increase promotes surface reactivity for subsequent fluorosilanization. The formation of siloxane (Si-O-Si) networks was also enhanced with longer plasma exposure, reflected by stronger bands near 1056 and 1011 cm^{-1}, corresponding to siloxane stretching vibrations [47], presented on figure 2(b). Notably, the differences between untreated, 1 min, and 4 min plasma-treated samples were more pronounced than between 4 and 10 min, suggesting that surface activation reaches a saturation point.

Samples activated by plasma for 1 min were silanized for 5 min and subsequently placed under vacuum for 5 or 10 min (figure 2(c)). The Si–O–Si stretching vibration increased after fluorosilanization, but decreased again after vacuum exposure, as highlighted in figure 2(c), indicating removal of loosely bound fluorosilanes. Similarly, C–F peaks weakened with longer vacuum, confirming the loss of physisorbed fluorosilane species in figure 2(e). The Si–O–Si changes can be attributed to fluorosilane molecules that reacted with each other through the free Si–OH groups, as reduced Si–OH content is observed with increasing fluorosilane treatment time. These results suggest that, while fluorosilanization increases Si–O–Si crosslinking through surface and self-condensation reactions, the subsequent vacuum step removes loosely bound or physisorbed fluorosilanes, including fluorinated residues. This implies that vacuum treatment enhances surface stability by leaving behind a more covalently anchored monolayer and reducing potential interference of unbound fluorosilane with MDX4 curing.

To further assess the influence of longer processing durations, we extended the fluorosilanization to 30 min and applied vacuum for 20 or 70 min (figure S3 in SM). These conditions amplified the observed trends: samples treated for 30 min showed strong CF_2 and CF stretching bands (1195, 1239 and 1144 cm^{-1}), which were progressively reduced as the vacuum

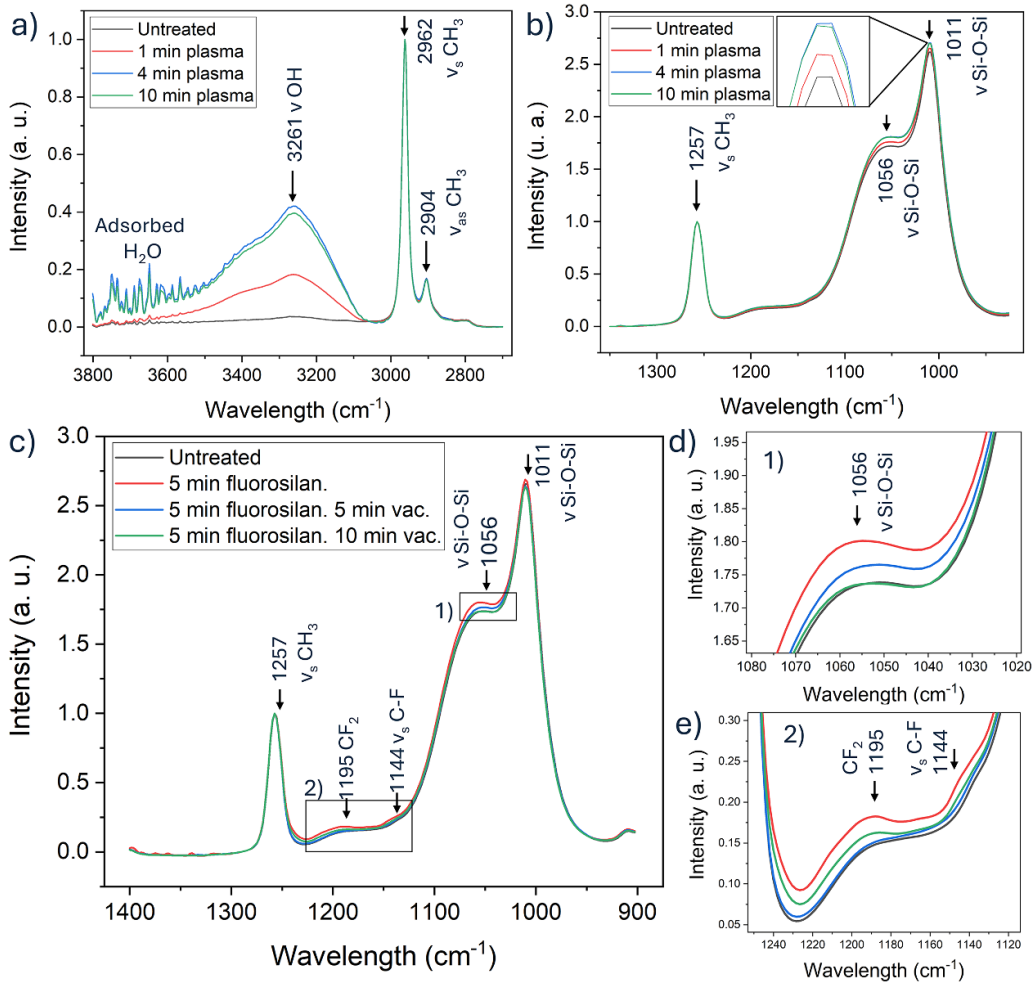

Figure 2. Fourier-transform infrared (FTIR) spectroscopy analysis of Sylgard 184 films subjected to different plasma activation and fluorosilanization conditions. (a) Scan showing OH stretching region (3100–3600 cm^{-1}) and CH stretching modes (2850–3000 cm^{-1}) for untreated surface and plasma treatment for 1, 4 and 10 min.(b) Si-O-Si and CH_3 stretching modes in the fingerprint region; inset highlights spectral shifts due to increasing plasma exposure. (c) Comparison of untreated and silanized samples with and without vacuum post-treatment for 5 and 10 min, showing peaks associated with fluorinated groups (CF_2 and CF_3). (d) Zoom into Si-O-Si peak region showing a change in peak intensity at 1056 cm^{-1} depending on treatment (region 1). (e) Zoom into CF vibration bands (region 2), showing diminishing intensity of fluorinated residues after vacuum treatment.

time increased. Similarly, the Si–O–Si signal at 1056 cm^{-1} decreased in the 70 min vacuum sample, indicating further removal of loosely bound fluorosilane species. Together, these results indicate the effect of vacuum treatment in reducing physisorbed fluorosilane residues and stabilizing the surface chemistry, which may help mitigate MDX4 curing inhibition and microstructure collapse during molding.

To analyze how the mold treatment influences the pillar fidelity, each treatment condition was applied to several molds. For each group, two sets of micropillared samples were produced: one immediately after the surface treatment (first demolding), and the second after reusing the same mold without reapplication of the surface treatment (second demolding). The structural fidelity of the resulting micropillars was assessed by quantifying the percentage of upright pillars using optical microscopy. Representative images from the first and second demolding of the pillars are shown in figures 3(a) and 3(b), respectively. Multiple randomly selected fields of view were analyzed for each sample, and the fraction of upright pillars are quantitatively described in 3(c).

We show that the surface treatment of Group 1 results in the largest amount of upright pillars after the first demolding, while Group 4 has the lowest fraction of upright pillars. Games-Howell tests reveal significant differences for the pillar fidelity after the first demolding between Group 1 and 2 ($t = 4.86, p = 0.001$), Group 1 and 4 ($t = 6.69, p = 0.0004$), Group 2 and 3 ($t = 3.615, p = 0.0014$) and Group 3 and 4 ($t = 5.310$, 0.0014) but not for the other comparisons ($p > 0.11$).

While plasma activation is commonly used to enhance fluorosilane bonding by increasing the density of hydroxyl groups, our results showed that its use was associated with lower replication fidelity (Groups 2 and 4). We hypothesize that overactivation of the mold surface may lead to excessive or unstable silane layers, potentially interfering with curing

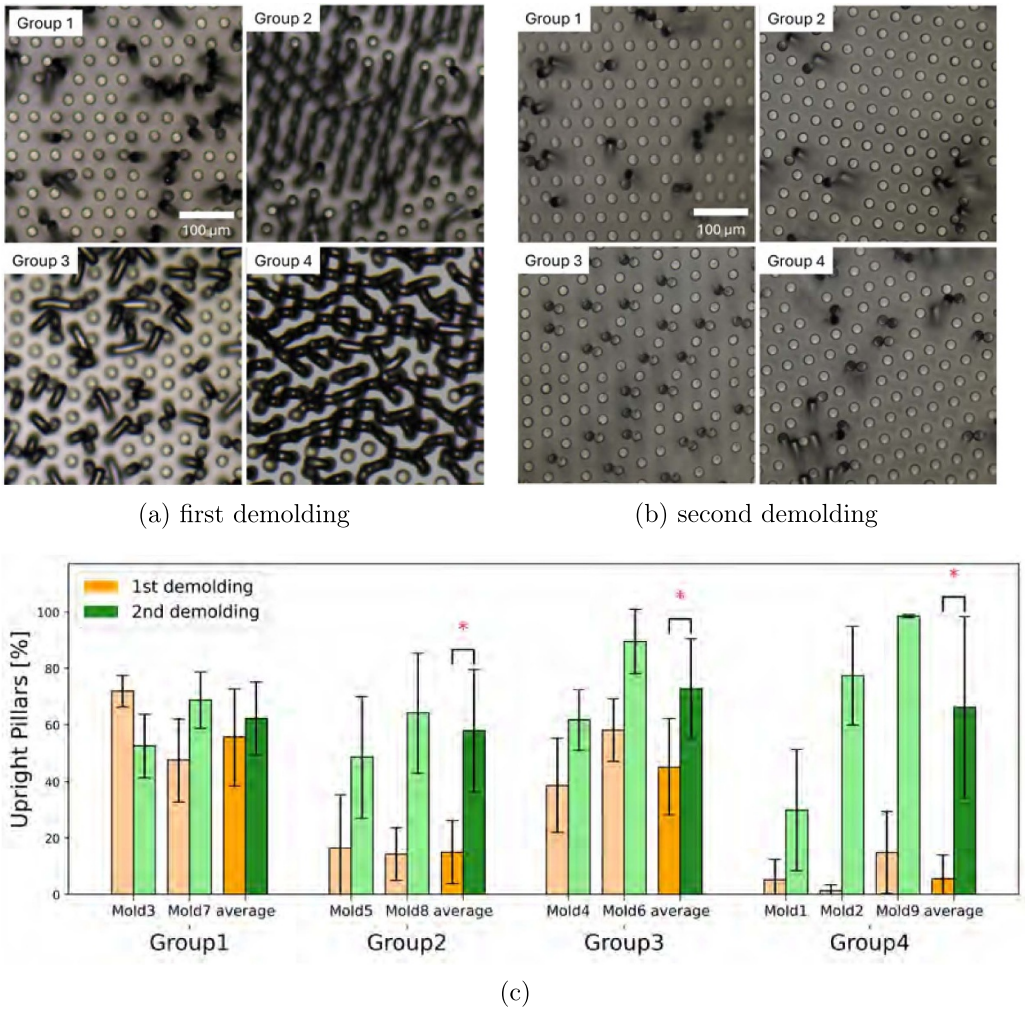

Figure 3. Evaluation of micropillar integrity for all four different surface treatment conditions applied to negative Sylgard molds for the first and second demolding. Representative sections of optical microscopy images from the first demolding for Groups 1–4 are shown in (a) and for the second in (b). (c) Quantitative analysis of the percentage of upright pillars for each treatment group, comparing first (orange) and second (green) demolding. Data represents mean ± sd across multiple images for individual molds of the groups (lighter colors) and for group average.

or demolding. Additionally, although less likely, plasma may introduce surface roughness or defects in PDMS molds, which could compromise mechanical stability during replication.

Significant improvements in pillar fidelity from the first to the second demolding were observed in Groups 2, 3, and 4 ($p < 0.05$). Although Group 1 did not show a statistically significant difference ($p = 0.4345$), the average still increased, indicating a positive trend. Overall, these results suggest that pillar fidelity generally improves with the second demolding.

For the second demolding we did not observe significant differences among the four groups ($t \in (0.46, 1.7), p > 0.11$). The fidelity of the second molding does not depend on the surface treatments of the negative molds.

To evaluate the mechanical integrity of the replicated structures, we measured the elastic modulus of the pillars and the backing layer by nanoindentation in samples after first and second molding from all four surface treatment groups. The indentation-retraction curves recorded on the microstructure exhibit characteristic step-like detachment patterns that allow estimation of stiffness (k_1, see equation (1)) for individual pillars (see figure S4 in SM for representative force-displacement curves after first demolding on pillar surface and backing layer). The calculated results for the Young's modulus (E) are summarized in figure 4.

The measured Young's modulus of the pillars is surprisingly low in comparison to literature. In general we report significantly higher elastic modulus for the flat surfaces than for the pillars (Welch two sample t-test: first molding: $t = 6.7$, $p < 0.001$, second molding: $t = 5$, $p < 0.001$), which could indicate not fully cured MDX4 in the pillar. The elastic modulus of the flat surface of the first and second molding seems not to change (Welch two sample t-test, $t = -0.05$, $p = 0.48$) while the pillars of the second molding tend to be stiffer, however just missing significance levels with $t = -1.58$ and $p = 0.067$. The determination of the indentation modulus following the Oliver–Pharr method [38] and the

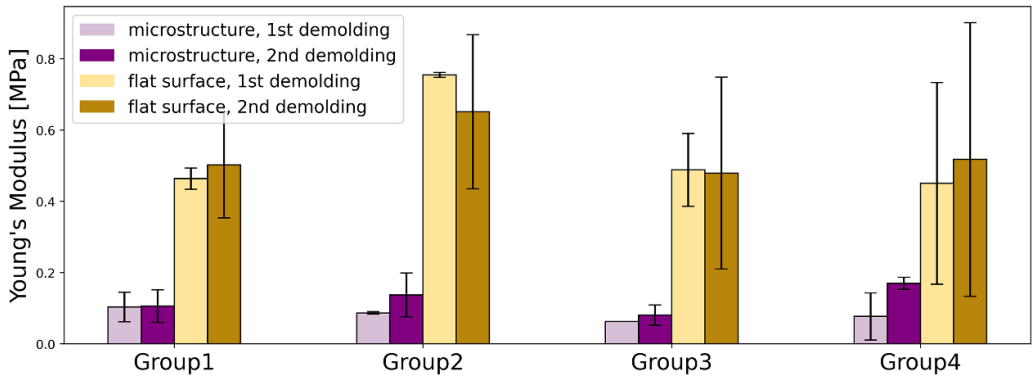

Figure 4. Comparison of Young's moduli obtained by nanoindentation on microstructured (purple) and flat (yellow) MDX4 surfaces. Lighter colors represent the modulus of the first demolded sample and darker colors indicate the second. Data represents mean ± sd across the different molds per group.

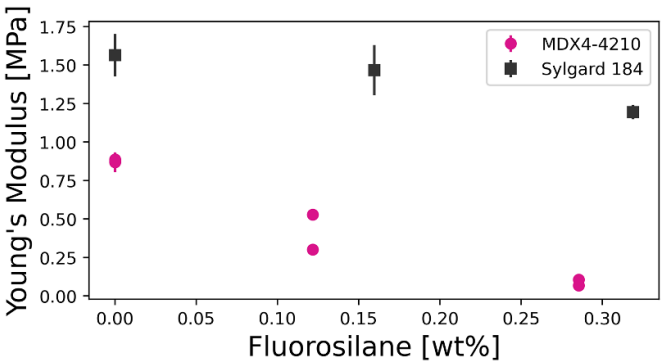

Figure 5. Young's modulus of MDX4- and Sylgard-based PDMS as a function of fluorosilane content in weight percent, added before curing. Data points represent mean values ± sd. Results for MDX4 are indicated by circles and for Sylgard by squares.

evaluation of pillar stretching [37] are both indirect methods for the determination of Young's modulus. However, both models attempt to reveal its value as closely as possible from experiments in geometries, where unidirectional deformation cannot be realized. We therefore trust that the surprisingly low value of Young's modulus for pillars is correct and performed the following experiment for an interpretation of the finding.

To explore whether the fluorosilane directly affects the stiffness of bulk MDX4, we systematically added controlled amounts of fluorinated silane into uncured MDX4 mixtures and measured the resulting elastic modulus of cylindrical MDX4 samples (diameter: 34 mm, height: 11.5 mm) after curing by uniaxial tensile tests. The resulting stress–strain curves show a clear reduction in Young's modulus with increasing fluorosilane concentration (see figure 5), indicating that residual fluorosilane can significantly reduce crosslinking density and, consequently, material stiffness. Even small additions (0.1%–0.3% fluorosilane-to-MDX4 by weight) led to a noticeable drop in stiffness, with values falling below 0.5 MPa for higher concentrations.

Control samples prepared with Sylgard exhibited significantly higher modulus values, as expected, and at all amounts of added fluorosilane. Again we observe lower Young's modulus for samples with fluorosilane addition. These results confirm that fluorosilane contamination in the mold or during processing can contribute to curing inhibition and softening of PDMS, which reinforces the importance of reducing fluorosilane carryover during replica molding.

As a complement to nanoindentation and tensile testing, Brillouin microscopy was employed to probe the local mechanical properties of upright and collapsed micropillars. To exemplify the differences in elasticity distributions between these two states, we selected a sample obtained from the second demolding of a mold treated according to Group 1.

Figure 6(a) shows a high-resolution map of the Brillouin shift for the axial plane of an upright pillar. A cross-section of the values along the center axis of the micropillar is provided in figure 6(b) in comparison to a parallel cross-section through the immersion liquid. The strong contrast in Brillouin shift between MDX4 and the surrounding immersion liquid reveals the shape of the micropillar. Rayleigh scattering at the interface between pillar and immersion liquid is minimized by the close matching of refractive index between the cured MDX4 ($n \approx 1.41$) and the immersion liquid (Immersol™ Sil 406, $n = 1.406$). This index matching minimizes optical discontinuities and supports accurate Brillouin shift measurements.

The length of this micropillar is about 70 μm and thus longer than the measured average pillar height of 62.09 μm on the master structure. Furthermore, the pillar diameter appears smaller than the original 18.95 μm. This observation is confirmed in a horizontal cross-section along the median plane of a group of pillars (figure S5 in SM). Measurements of 35 randomly selected pillars on several samples from different treatment groups reveal a pillar height up to 68.7 μm and a diameter down to 15.5 μm. This elongation of micropillars was found on some but not all other samples, irrespective of the previous mold treatment (average over all measured pillars—height: 63.9 ± 3.29 μm, diameter: 17.53 ± 1.46 μm). We suggest that the demolding process caused significant stretching of the not fully cured pillars, and that those pillars do not return to the shape of the original structure, indicating plastic deformation.

Variations of the Brillouin shift within the pillars indicate inhomogeneities of the mechanical properties. The Brillouin

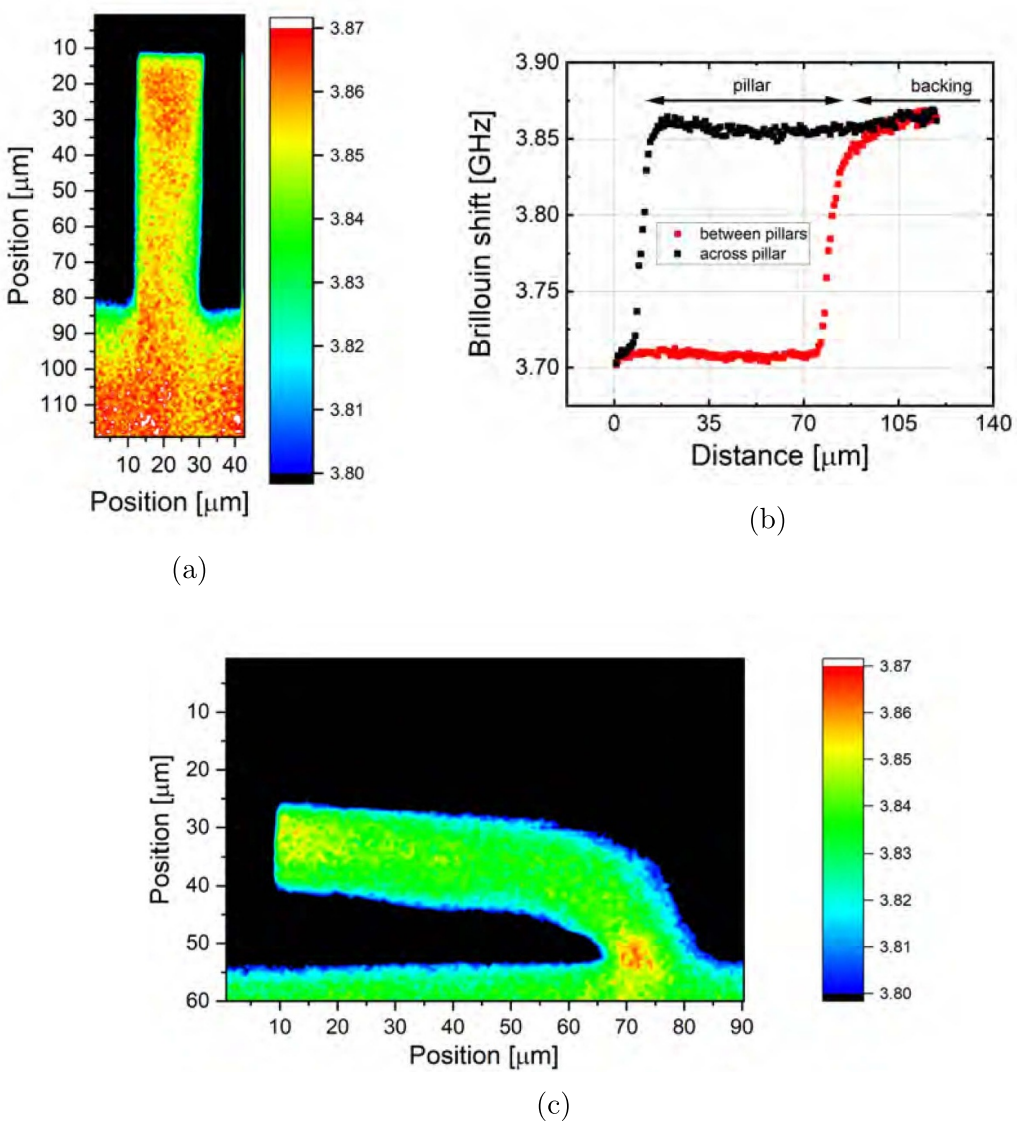

Figure 6. Brillouin microscopy of micropillars from a sample produced in the second demolding from a mold of Group 1. (a) High-resolution Brillouin shift map of the axial plane of an upright pillar, highlighting its elongation and spatial variations in local stiffness. (b) Brillouin shift profile extracted along the center axis of the same pillar in comparison to a profile taken between pillars. (c) High-resolution Brillouin shift map of a collapsed pillar.

shift is expected to scale with $\sqrt{M/\rho}$, where M is the longitudinal modulus at GHz frequencies and ρ is the density of the material. If we interpret lower shifts as a weakening of the material, we observe in figure 6(a) that this pillar is weakened in its lower half, in particular close to the surface. Similarly, the surface of the backing layer is weakened. This finding is in agreement with the suggested softening of MDX4 by the fluorosilane film on the mold. Please note that the depth of weakening is larger than the method's resolution of 1 μm in lateral and 4 μm in vertical direction [40].

Figure 6(c) reveals the Brillouin shift across a collapsed pillar. An overall Brillouin shift is lower than the one in the upright pillar from the same sample in figure 6(a), indicating a overall lower modulus as cause for the collapse. A similar weakening in the lower half of the pillar is found. The local maximum of the Brillouin shift at the sharpest bending point probably originates in local compressive strain, which increases the Brillouin shift of elastomers [48]. Results of the Brillouin microscopy thus provide further evidence for a variation of mechanical properties among micropillars, support the notion of a mechanical softening of MDX4 by contact to the fluorosilane layer on the mold, and additionally indicate that micropillars are prone to an irreversible elongation in the process of unmolding. Our hypothesis about incomplete curing, which was based on nanoindentation, and mechanical testing results is thus confirmed as mechanical inhomogeneity in collapsed pillars revealed by Brillouin Microscopy.

4. Conclusions

We have systematically investigated the role of surface treatment in replica molding of high-aspect-ratio micropillars

using a soft biomedical-grade elastomer (MDX4). Our results highlight several important findings that inform best practices for replication:

- The inclusion of a vacuum step after fluorosilanization reduces unbound fluorosilane residues on the mold surface, but this did not translate into a higher fraction of upright structures. Instead, we found that producing a sacrificial first molding consistently improved the fidelity of subsequent replications, regardless of the initial surface treatment protocol. This suggests that the first replication removes loosely bound or excess fluorosilane that would otherwise interfere with MDX4 crosslinking.
- Nanoindentation tests revealed lower Young's modulus values for the micropillars compared to flat films of the same material, consistent with reduced mechanical stability of the replicated structures. While only upright pillars were measured, we hypothesize that insufficient stiffness contributes to the observed lateral collapse [27]. However, no significant difference in modulus was found between samples from first and second demolding, despite a clear improvement in structural fidelity after reuse. From Brillouin microscopy, we observed that an upright pillars exhibited higher Brillouin shifts than a collapsed one, indicating a stiffer material at least at GHz frequencies tested by the method. Furthermore, pillars can be irreversibly elongated in demolding and show a weakening starting from surfaces in contact with the mold. These findings confirm that factors beyond bulk stiffness, such as changes in mold surface chemistry or fluorosilane removal, play a critical role in successful replication.
- Direct mixing experiments demonstrated that even small concentrations of fluorosilane significantly reduce the elastic modulus of cured PDMS, further reinforcing the need to control fluorosilane exposure during the molding process.

Taken together, these findings show the importance of mold surface chemistry in achieving high-fidelity micropillar arrays using soft elastomers. By implementing a sacrificial molding step, more robust and reproducible micropillar arrays can be produced, an essential requirement for applications in biomedical devices, adhesives, and soft robotics.

Despite its advantages, the proposed strategy also presents certain limitations. It currently relies on relatively simple micropillar geometries and requires multiple demolding steps. While the method is effective for soft PDMS systems, its compatibility with other polymer formulations or extreme aspect ratios remains to be further validated. The long-term stability of the reusable molds after multiple cycles were not explored in this work and is an important topic for future investigation.

Data availability statement

The data cannot be made publicly available upon publication because they are not available in a format that is sufficiently accessible or reusable by other researchers. The data that support the findings of this study are available upon reasonable request from the authors.

Additional characterization available at https://doi.org/10.1088/1361-6439/ae1e87/data1.

Acknowledgments

The authors would like to acknowledge Pamela Kalmes for the assistance in preparing samples, Fabian Faller for the assistance with nanoindentation measurements, and Robert Drumm for assistance with the UPM measurements. The research leading to these results has received funding from the European Research Council under the European Union's HORIZON-EU.1.1 program/ERC PoC Grant Agreement No. 842 613, Advanced Grant 'Stick2Heal' to E A and from the Volkswagen Foundation.

Conflict of interest

RS and TJ are employees of CellSense GmbH, the manufacturer of the CellSense Discoverer Brillouin microscope used in this study. They may have a financial interest in the commercialization of this technology. The other authors declare no competing interests.

Author contributions

Gabriela Moreira Lana 0000-0002-8346-6951
Conceptualization (equal), Investigation (equal), Writing – original draft (equal), Writing – review & editing (equal)

Maja Fehlberg 0000-0002-1827-2333
Conceptualization (equal), Investigation (equal), Writing – original draft (equal), Writing – review & editing (equal)

Petra Herbeck-Engel
Investigation (equal), Writing – review & editing (equal)

Gisela Heppe
Investigation (equal), Writing – review & editing (equal)

Raimund Schlüßler 0000-0003-3752-2382
Investigation (equal), Writing – review & editing (equal)

Torsten Jähnke 0009-0008-7343-7082
Investigation (equal), Writing – review & editing (equal)

Eduard Arzt
Resources (equal), Writing – review & editing (equal)

Roland Bennewitz 0000-0002-5464-8190
Conceptualization (equal), Resources (equal), Writing – original draft (equal), Writing – review & editing (equal)

References

[1] Arzt E, Quan H, McMeeking R M and Hensel R 2021 Functional surface microstructures inspired by nature–from adhesion and wetting principles to sustainable new devices *Prog. Mater. Sci.* **119** 1–105

[2] Zhang X, Wang Y, Hensel R and Arzt E 2021 A design strategy for mushroom-shaped microfibrils with optimized

dry adhesion: experiments and finite element analyses *J. Appl. Mech. - Trans. ASME* **88** 1–9
[3] Hensel R, Moh K and Arzt E 2018 Engineering micropatterned dry adhesives: from contact theory to handling applications *Adv. Funct. Mater.* **28** 1800865
[4] He Z, Moyle N M, Hui C Y, Levrard B and Jagota A 2017 Adhesion and friction enhancement of film-terminated structures against rough surfaces *Tribol. Lett.* **65** 1–8
[5] Hansen C J, Saksena R, Kolesky D B, Vericella J J, Kranz S J, Muldowney G P, Christensen K T and Lewis J A 2013 High-throughput printing via microvascular multinozzle arrays *Adv. Mater.* **25** 96–102
[6] Cho S H *et al* 2025 Soft, wearable, microfluidic system for fluorometric analysis of loss of amino acids through eccrine sweat *Lab Chip* **25** 1647–55
[7] Khot M I *et al* 2020 Characterising a PDMS based 3D cell culturing microfluidic platform for screening chemotherapeutic drug cytotoxic activity *Sci. Rep.* **10** 15915
[8] Alghannam F, Alayed M, Alfihed S, Sakr M A, Almutairi D, Alshamrani N and Fayez N A 2025 Recent progress in PDMS-based microfluidics toward integrated organ-on-a-chip biosensors and personalized medicine *Biosensors* **15** 76
[9] Lana G M, Zhang X, Müller C, Hensel R and Arzt E 2022 Film-terminated fibrillar microstructures with improved adhesion on skin-like surfaces *ACS Appl. Mater. Interfaces* **14** 46239–51
[10] Fehlberg M, Kim K S, Drewing K, Hensel R and Bennewitz R 2022 Perception of friction in tactile exploration of micro-structured rubber samples *Haptics Sci., Technol. Appl.* **13325** 21–9
[11] Song E *et al* 2021 Miniaturized electromechanical devices for the characterization of the biomechanics of deep tissue *Nat. Biomed. Eng.* **5** 759–71
[12] Chan E P, Greiner C, Arzt E and Crosby A J 2007 Designing model systems for enhanced adhesion *MRS Bull.* **32** 496–503
[13] Zhuang G and Kutter J P 2011 Anti-stiction coating of pdms moulds for rapid microchannel fabrication by double replica moulding *J. Micromech. Microeng.* **21** 105020
[14] Poon J K S, Huang Y, Paloczi G T and Yariv A 2004 Soft lithography replica molding of critically coupled polymer microring resonators *IEEE Photonics Technol. Lett.* **16** 2496–8
[15] Pan Z, Shahsavan H, Zhang W, Yang F K and Zhao B 2015 Superhydro-oleophobic bio-inspired polydimethylsiloxane micropillared surface via fdts coating/blending approaches *Appl. Surf. Sci.* **324** 612–20
[16] Moresco J, Clausen C H and Svendsen W 2010 Improved anti-stiction coating of SU-8 molds *Sens. Actuators B* **145** 698–701
[17] Gilles S 2007 Chemical modification of silicon surfaces for the application in soft lithography *Thesis* Forschungszentrum Jülich Jülich, Germany
[18] Lessel M Bäumchen O, Klos M, Hähl H, Fetzer R, Paulus M, Seemann R and Jacobs K 2015 Self-assembled silane monolayers: an efficient step-by-step recipe for high-quality, low energy surfaces *Surf. Interface Anal.* **47** 557–64
[19] Munief W-M, Heib F, Hempel F, Lu X, Schwartz M , Pachauri V, Hempelmann R, Schmitt M and Ingebrandt S 2018 Silane deposition via gas-phase evaporation and high-resolution surface characterization of the ultrathin siloxane coatings *Langmuir* **34** 10217–29
[20] Beck M , Graczyk M, Maximov I, Sarwe E-L, Ling T G I, Keil M and Montelius L 2002 Improving stamps for 10 nm level wafer scale nanoimprint lithography *Microelectron. Eng.* **61–62** 441–8
[21] Hartmann M R 2020 Wetting states of droplets on patterned surfaces and in an electric field *Phd Thesis* TU Darmstadt
[22] Egghe L, Kaiser J, Geisel K, Schimmel T and del Campo A 2022 Plasma treatment protocols and their impact on surface chemistry and reproducibility for PDMS silanization *ACS Appl. Mater. Interfaces* **14** 45586–98
[23] Huang Y, Ogaki R, Andresen T L and Dufva M 2024 Plasma-mediated silanization for bonding PDMS to glass: a simplified protocol for long-lasting surface activation *Sci. Rep.* **14** 468
[24] Schade M, Franzka S, Schröter A, Cappuccio F, Gajda M, Peinecke V, Heinzel A and Hartmann N 2014 Chemical functionalization of carbon/polymer bipolar plate materials via oxygen plasma activation and subsequent silanization *Surf. Coat. Technol.* **240** 255–60
[25] Langowski B A and Uhrich K E 2005 Oxygen plasma-treatment effects on Si transfer during microcontact printing *Langmuir* **21** 6366–72
[26] Ashurst W R, Carraro C and Maboudian R 2003 Vapor phase anti-stiction coatings for MEMS *IEEE Trans. Device Mater. Reliab.* **3** 173–8
[27] Glassmaker N J, Jagota A, Hui C Y and Kim J 2004 Design of biomimetic fibrillar interfaces: 1. making contact *J. R. Soc. Interface* **1** 23–33
[28] Papadopoulos P *et al* 2018 Recovery of collapsed PDMS micropillar arrays using ultrasonic agitation and ethanol rinsing *Microsyst. Technol.* **24** 4339–46
[29] Sáez J *et al* 2010 Soft lithography for creating PDMS microfluidic devices: methods and challenges *Lab Chip* **10** 1551–5
[30] Wang D, Zhuang M and Tian X 2023 Effectiveness of organic solvents for recovering collapsed PDMS micropillar arrays *RSC Adv.* **13** 4874–9
[31] Zhang Y, Chi-Wei Lo J A T and Yang S 2006 Replica molding of high-aspect-ratio polymeric nanopillar arrays with high fidelity *Langmuir* **22** 8595–601
[32] Finn M *et al* 2013 Collapse and recovery of high aspect ratio PDMS micropillar arrays *J. Micromech. Microeng.* **23** 125007
[33] Park S-H, Kim K H, Lim T W, Yang D-Y and Lee K-S 2008 Investigation of three-dimensional pattern collapse owing to surface tension using an imperfection finite element model *Microelectron. Eng.* **85** 432–9
[34] Amato L, Keller S S, Heiskanen A, Dimaki M, Emnéus J, Boisen A and Tenje M 2012 Fabrication of high-aspect ratio SU-8 micropillar arrays *Microelectron. Eng.* **98** 483–7
[35] Eren E *et al* 2025 Material stiffness influences collapse behavior of 3d-printed micropillars fabricated by two-photon polymerization *Addit. Manuf.* **45** 103152
[36] Johnston I D, McCluskey D K, Tan C K L and Tracey M C 2014 Mechanical characterization of bulk Sylgard 184 for microfluidics and microengineering *J. Micromech. Microeng.* **24** 035017
[37] Guidoni G M, Schillo D, Hangen U, Castellanos G, Arzt E, McMeeking R M and Bennewitz R 2010 Discrete contact mechanics of a fibrillar surface with backing layer interactions *J. Mech. Phys. Solids* **58** 1571–81
[38] Kan Q, Yan W, Kang G and Sun Q 2013 Oliver–Pharr indentation method in determining elastic moduli of shape memory alloys–a phase transformable material *J. Mech. Phys. Solids* **61** 2015–33
[39] Scarcelli G and Yun S H 2008 Confocal Brillouin microscopy for three-dimensional mechanical imaging *Nat. Photon.* **2** 39–43
[40] Schlüßler R *et al* 2022 Correlative all-optical quantification of mass density and mechanics of subcellular compartments with fluorescence specificity *eLife* **11** e68490
[41] Fischer S C L , Groß K, Torrents Abad O, Becker M M, Park E, Hensel R and Arzt E 2017 Funnel-shaped

microstructures for strong reversible adhesion *Advanced Materials Interfaces* **4** 1700292
[42] Lana G M, Sorg K, Wenzel G I, Hecker D, Hensel R, Schick B, Kruttwig K and Arzt E 2021 Self-adhesive silicone microstructures for the treatment of tympanic membrane perforations *Adv. NanoBiomed. Res.* **1** 2100057
[43] Yuxin Li *et al* 2023 Functional PDMS elastomers: bulk composites, surface engineering and precision fabrication *Adv. Sci.* **10** 2207523
[44] Waddell E A, Shreeves S, Carrell H, Perry C, Reid B A and McKee J 2008 Surface modification of Sylgard 184 polydimethylsiloxane by 254 nm excimer radiation and characterization by contact angle goniometry, infrared spectroscopy, atomic force and scanning electron microscopy *Appl. Surf. Sci.* **254** 5314–8
[45] Bodas D, Rauch J-Y and Khan-Malek C 2008 Surface modification and aging studies of addition-curing silicone rubbers by oxygen plasma *Eur. Polym. J.* **44** 2130–9
[46] Efimenko K, Wallace W E and Genzer J 2002 Surface modification of Sylgard-184 poly(dimethyl siloxane) networks by ultraviolet and ultraviolet/ozone treatment *J. Colloid Interface Sci.* **254** 306–15
[47] Mata A, Fleischman A J and Roy S 2005 Characterization of polydimethylsiloxane (PDMS) properties for biomedical micro/nanosystems *Biomed. Microdevices* **7** 281–93
[48] Stevens L L, Orler E B, Dattelbaum D M, Ahart M and Hemley R J 2007 Brillouin-scattering determination of the acoustic properties and their pressure dependence for three polymeric elastomers *J. Chem. Phys.* **127** 104906